Preprint of the article: https://doi.org/10.1109/AIRPHARO52252.2021.9571054
Nekoo, Saeed Rafee, et al. "Experimental Investigation of Soft-Landing of Quadrotors via Induced Wind Modeling Approach." *2021 Aerial Robotic Systems Physically Interacting with the Environment (AIRPHARO)*. IEEE, 2021.

Experimental Investigation of Soft-Landing of Quadrotors via Induced Wind Modeling Approach

Saeed Rafee Nekoo, Pedro J. Sanchez Cuevas, José Ángel Acosta, Guillermo Heredia and Anibal Ollero

***Abstract*—This paper presents an experimental study of the soft-landing problem in quadrotors using the induced wind modeling approach. The landing phase has been typically one of the critical phases in drone flight. Landing complexity drastically increases when the drone needs to land on sensitive sites, such as platforms or rack of pipes in refineries (for inspection purposes), in which explosive material is running through or there exist flammable/explosive material in the environment. Multirotor unmanned aerial vehicles (UAVs) are usually lightweight platforms and they are significantly disturbed by the aerodynamic ground effect while landing; so, near the ground, those drones are subjected to an external disturbance in proximity to the ground. In this situation, the airflow can be reflected after reaching the ground, disturbing the performance of the rotors significantly. This paper aims to model the induced wind velocity, caused by the propellers to see and consider the ground effect during the landing. The reduction of the total thrust near the ground provides a smooth landing and avoids bumping. The complex wind modeling formulation and limitation of the commercialized autopilots make the implementation a challenging task. Herein we propose how to incorporate the proposed soft-landing algorithm within an existing UAV autopilot. Experimental results show that the proposed approach successfully replicates the wind modeling which leads to a soft-landing.**

I. Introduction

Inspection and Maintenance (I&M) is an essential task for industrial plants and big companies. This task aims to keep the infrastructure operational as much time as possible and predict the failures in the system before they arise. An oil refinery is one case that needs monitoring and inspection periodically; i.e. inspection of the thickness of the pipes [1]. The HYFLIERS (HYbrid FLying-rollIng with-snakE-aRm robot for contact inSpection) project aims to include drones as an enabling technology to facilitate and accelerate I&M operations reducing risks and costs [2]. Oil and gas plants are varied environments with kilometers of long-isolated pipes and racks of pipes. The massive length of the pipelines is enough to justify the cost of an automated system for I&M. We narrow our research, focusing on landing on a platform or a rack of pipes (pipes arranged close together) for two reasons: 1) This is one of the most common structures of oil and gas plants and 2) the aerodynamic problem is very similar to the problem of landing on the ground. In those environments, the landing must be soft/smooth without any bumps or hard contact to avoid generating damage to the infrastructure. This has been previously studied using a specific physical landing gear under a drone to provide that condition. Luo et al. presented a soft-landing gear, fabricated by Elastosil M4601 silicone material, like four soft fingers to clamp around a pipe [3]. They also used a neural network controller to design avian landing behavior on non-flat surfaces. Sahinoz proposed and analyzed a landing gear for the soft landing of a lunar lander [4]. The rover lander's weight was significant and obliged the designers to use a stable soft-landing gear to maintain structural integrity. Zhang et al. presented a bioinspired landing gear for a soft touch down in the landing phase [5]. The landing was considered between 1 to 2 (m/s); using a shock absorber and parallel flexible mechanism design, the system could be successfully landed. Hang et al. presented a multimodal landing/perching gear for a multirotor unmanned aerial vehicle [6]. They presented a modularized and actuated landing gear framework that worked with different scenarios and structures. Using an air damper and elastic structure were also reported for absorbing the shock during the landing phase [7].

In this work, we approach the soft-landing subject in terms of control design, without adding physical landing gear under a drone. The objective is to obtain a controlled smooth landing maneuver without increasing the complexity and the total weight of the aerial system. Avoiding hard impact with a specific control strategy has been previously studied in many other applications such as electromechanical valves [8]. Peterson and Stefanopoulou proposed a control approach, extremum seeking, to reduce the speed of the impact, then having a better smooth landing [8]. Yang and Baoyin presented a fuel-optimal control method for soft-landing on a moving object [9]. Mercorelli used adaptive control for a soft-landing of electromagnetic actuators [10]. A pre-action was done to avoid saturation and then hard impact by the electromagnetic input, in order to change the plant. Nevertheless, the slow or controlled landing must be gained utilizing proper feedback and precise control. Myeong and Myung presented a wall climbing drone for soft-landing [11]. Fricke et al. used a machine learning approach for vertical soft landing [12].

Regarding the aerodynamic problem, the ground effect has been extensively studied in the literature. The classic method was presented by Cheeseman and Bennet, using the assumptions of

This work is supported by the HYFLIERS project (HYbrid FLying-rolling with-snakE-aRm robot for contact inspection) funded by the European Commission H2020 Programme under grant agreement ID: 779411 (https://cordis.europa.eu/project/rcn/213049)] and by the ARTIC project funded by the Ministerio de Ciencia, Innovación y Universidades under the grant agreement ID: RTI2018-102224-B-I00.

S. R. Nekoo, J. Á. Acosta, G. Heredia and A. Ollero are with GRVC Robotics Lab., Universidad de Sevilla, Seville, Spain; e-mails: saerafee@yahoo.com, {jaar, guiller, aollero}@us.es.

P.J. Sanchez-Cuevas is with SpaceR Research Group, SnT - University of Luxembourg, pedro.sanchezcuevas@uni.lu.

Preprint of the article: https://doi.org/10.1109/AIRPHARO52252.2021.9571054
Nekoo, Saeed Rafee, et al. "Experimental Investigation of Soft-Landing of Quadrotors via Induced Wind Modeling Approach." *2021 Aerial Robotic Systems Physically Interacting with the Environment (AIRPHARO)*. IEEE, 2021.

the linearized potential aerodynamics [18]. Since then, several studies have been accomplished so far to model this aerodynamic problem in helicopters [13-15], and the extension of that idea for quadrotors [16-19].

Recently, the use of neural networks has been also reported for learning the complex aerodynamics effect near the ground [20]. They performed deep learning based on nonlinear control with guaranteed stability. The combination of neural networks, intelligent control, and inverse dynamics was also used for landing [21]. The induced wind under a multirotor drone generates disturbance near the ground, which is so-called the ground effect [18]. It was studied and modeled in terms of thrust (force) for a single propeller [22], and also for a quadrotor [18]. The method of the images of Betz was used to deliver a relation for computation of the reflected thrust. That defined the reflected wind produced by the propellers which imposed on the unmanned aerial vehicle (UAV) additional thrust. If one neglects this additional thrust, the UAV faces a couple of bumps before landing (or before turning off the rotors). Here we approach the issue differently. We compute the induced wind speed using an augmented model of flying objects that includes external wind gusts. Lungu proposed this modeling for fixed-wing unmanned aerial vehicles during landing and the source of the wind was completely external from the environment [23]. We use the same model; however, the wind is caused by the drone's propellers, as a reflection near the ground.

This approach is subjected to uncertainty in modeling, aerodynamics, wind reflection, and the nonlinearity of the platform itself. A robust controller is required to control the system, i.e. the sliding mode control (SMC); previously employed for simulation study and modeling of the system [24]. On the one hand, modifying the autopilots of commercial drones is not possible in some cases (to implement complex controllers such as SMC). On the other hand, end-users prefer commercial drones for the sake of repairs, an extension of the service fast by increasing the number of drones, etc. So, implementation of the soft-landing approach is required on the standard autopilots. They use PD/PID control, and implementing the proposed soft-landing approach on them is a challenge.

The main contribution of this work is the experimental implementation of the proposed soft-landing approach adapted to commercial autopilots. Concerning previous work Ref. [24], which was a purely theoretical work, this current paper implements the soft-landing method experimentally and briefly reports it. The comparison of the landing with/without the algorithm validates the effectiveness of the method.

The rest of the work is structured as follows. Section II briefly expresses the system modeling: induced wind velocity, ground effect, and quadrotor dynamics. Section III introduces the platform and experimental setup characteristics. Section IV shows the results and Section V presents the concluding remarks.

II. System Modeling

A. Induced wind velocity

The momentum theory must be revisited to define the induced wind velocity of the propellers under the quadrotor drone. Considering a single propeller, passing the air through, please see Fig. 1, the existence of the following conditions are assumed [25]: the velocity is constant over the disc, the pressure is uniform over the disc, rotation imparted to the flow as it passes through the propeller is neglected, the flow pass through the propeller can be separated from the rest of the flow by a well-defined stream tube, and the flow is incompressible.

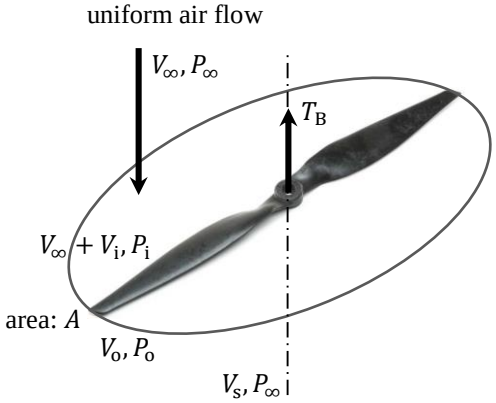

Fig. 1. Description of the momentum theory on a propeller.

$V_\infty \left(\frac{m}{s}\right)$ is the velocity of airflow in front of the propeller, far from the propeller, and V_i close to that, V_o is a velocity closely behind the propeller and V_s an ultimate downstream velocity of the airflow. The pressure is presented by P (Pa), with indices "∞" denotes the environment, "i" in-front and "o" behind the propeller with respect; the area of the rotating propeller is shown by A (m^2). The thrust, T_B (N), is shaped by $T_B = A(P_o - P_i)$. Using conversion of the mass, in-front and behind the propeller, and thrust relation, also mathematical manipulation, one could find the induced wind velocity in terms of thrust [25]:

$$V_i = -\frac{V_\infty}{2} + \sqrt{\frac{V_\infty^2}{4} + \frac{T_B}{2\rho A}}, \quad (1)$$

$$V_o = \frac{V_\infty}{2} + \sqrt{\frac{V_\infty^2}{4} + \frac{T_B}{2\rho A}}, \quad (2)$$

where $\rho \left(\frac{kg}{m^3}\right)$ is the air density.

B. Ground effect

Considering the environmental wind speed zero, $V_\infty = 0$, the thrust of one propeller is found using Eq. (1) or (2), $T_B = 2\rho A V_o^2$. The ground effect for propeller systems was proposed to define a relation for calculating the thrust near the ground based on the image method [22, 26]. The reflective thrust for a single propeller is [26]:

$$\frac{T_g}{T_B} = \frac{1}{1 - \left(\frac{R}{4z_c}\right)^2}, \quad (3)$$

where T_B (N) is the thrust of the free flight, T_g (N) is the thrust under the ground effect, R (m) is the radius of the propeller and

Preprint of the article: https://doi.org/10.1109/AIRPHARO52252.2021.9571054
Nekoo, Saeed Rafee, et al. "Experimental Investigation of Soft-Landing of Quadrotors via Induced Wind Modeling Approach." *2021 Aerial Robotic Systems Physically Interacting with the Environment (AIRPHARO)*. IEEE, 2021.

z_c (m) is the distance of the rotor from the ground. Equation (3) is rewritten for a quadrotor as [18]:

$$\frac{T_g}{T_B} = \frac{1}{1-\left(\frac{R}{4z_c}\right)^2 - \frac{R^2 z_c}{\sqrt{(d+4z_c^2)^3}} - \frac{R^2 z_c}{2\sqrt{(2d+4z_c^2)^3}}}. \quad (4)$$

To transform (4) to an equation in terms of airflow velocity, the conversion between force and the mass flow rate is used [24]:

$$T_g = 2\rho A_o V_g^2, \quad (5)$$

$$T_B = 2\rho A_o V_o^2, \quad (6)$$

where $A_o = 4\pi R^2$ (m^2) is the area of four propellers. Substituting (5) and (6) in Eq. (4), one could represent the ground reflection of wind with direction towards the ground, $-Z$, which causes the negative sign for V_g:

$$V_g = -V_o \frac{1}{\sqrt{1-\left(\frac{R}{4z_c}\right)^2 - \frac{R^2 z_c}{\sqrt{(d+4z_c^2)^3}} - \frac{R^2 z_c}{2\sqrt{(2d+4z_c^2)^3}}}}. \quad (7)$$

The distance between the quadcopter and the ground for studying the ground effect was stated dist.$= 5R$ [18]. The control, using (7) is applicable, since V_g in reality is less than the theoretical estimation. The airflow speed by the ground is

$$\begin{cases} V_G = \frac{V_g}{5R} z_c - V_g, & z_c \in [0, 5R], \\ 0 & z_c > 5R. \end{cases} \quad (8)$$

Equation (8) implies that the high-speed reaction by the ground is generated near the ground and increases the thrust of the UAV.

C. Quadrotor dynamics

A moving coordinate (body frame) is attached to the center of mass of the quadrotor defined by $\{x_c, y_c, z_c\}$ that can move and rotate concerning inertial frame $\{X, Y, Z\}$, or Earth frame: Z axis is from the center of the earth to surface, Y axis pointing to the North and X axis pointing to the East. The generalized coordinates include the absolute position of the system and Euler angles for inertial frame $\mathbf{q}(t) = [\boldsymbol{\xi}_1^T(t), \boldsymbol{\xi}_2^T(t)]^T = [x_c(t), y_c(t), z_c(t), \phi(t), \theta(t), \psi(t)]^T$ (m, rad). The angular velocities of the body frame, linear and rotational, are expressed as [27]:

$$\boldsymbol{\upsilon}_1(t) = [u(t), v(t), w(t)]^T \left(\frac{\text{m}}{\text{s}}\right),$$

$$\boldsymbol{\upsilon}_2(t) = [p(t), q(t), r(t)]^T \left(\frac{\text{rad}}{\text{s}}\right).$$

The kinematics relations between the two reference frames are defined by [28]:

$$\dot{\boldsymbol{\xi}}_1(t) = \mathbf{R}_{ZYX}(\boldsymbol{\xi}_2(t))\boldsymbol{\upsilon}_1(t),$$

$$\dot{\boldsymbol{\xi}}_2(t) = \mathbf{T}(\boldsymbol{\xi}_2(t))\boldsymbol{\upsilon}_2(t),$$

in which $\mathbf{R}_{ZYX}(\boldsymbol{\xi}_2(t))$ is the rotation matrix and $\mathbf{T}(\boldsymbol{\xi}_2(t))$ relates the angular velocities between the two reference frames:

$$\mathbf{R}_{ZYX}(\boldsymbol{\xi}_2(t)) = \begin{bmatrix} c_\theta c_\psi & s_\phi s_\theta c_\psi - c_\phi s_\psi & c_\phi s_\theta c_\psi + s_\phi s_\psi \\ c_\theta s_\psi & s_\phi s_\theta s_\psi + c_\phi c_\psi & c_\phi s_\theta s_\psi - s_\phi c_\psi \\ -s_\theta & s_\phi c_\theta & c_\phi c_\theta \end{bmatrix},$$

$$\mathbf{T}(\boldsymbol{\xi}_2(t)) = \begin{bmatrix} 1 & s_\phi t_\theta & c_\phi t_\theta \\ 0 & c_\phi & -s_\phi \\ 0 & s_\phi / c_\theta & c_\phi / c_\theta \end{bmatrix}.$$

The state vector of the system is chosen

$$\mathbf{x}(t) = [\boldsymbol{\xi}_1^T(t), \boldsymbol{\xi}_2^T(t), \boldsymbol{\upsilon}_1^T(t), \boldsymbol{\upsilon}_2^T(t)]^T,$$

which results in the state-space representation of dynamics without modeling of wind:

$$\dot{\mathbf{x}} = \begin{bmatrix} \mathbf{R}_{ZYX}(\boldsymbol{\xi}_2)\boldsymbol{\upsilon}_1 \\ \mathbf{T}(\boldsymbol{\xi}_2)\boldsymbol{\upsilon}_2 \\ \mathbf{R}_{ZYX,3}(\boldsymbol{\xi}_2)\, T_B/m - \hat{\boldsymbol{\upsilon}}_2\boldsymbol{\upsilon}_1 - g\mathbf{e}_3 - \mathbf{D}\dot{\boldsymbol{\xi}}_1/m \\ \mathbf{I}^{-1}(\boldsymbol{\tau}_B - \hat{\boldsymbol{\upsilon}}_2\mathbf{I}\boldsymbol{\upsilon}_2) \end{bmatrix}. \quad (9)$$

This model is valid under hovering conditions that require small changes in orientation dynamics [29-31].

D. Wind modeling

The input information of the wind to the problem is the wind velocity in inertial coordinates, set by $\mathbf{W}(t) = [W_X(t), W_Y(t), W_Z(t)]^T$ (m/s). To transform the wind elements to the body frame, a rotation matrix is used; and we introduce the wind vector in the body coordinate:

$$\mathbf{W}_c(t) = \left[W_x(t), W_y(t), W_z(t)\right]^T = \mathbf{R}_{ZYX}^T(\boldsymbol{\xi}_2(t))\mathbf{W}(t)\left(\frac{\text{m}}{\text{s}}\right).$$

Considering the wind, the modified form of state-space equation (9) is [32]:

$$\dot{\mathbf{x}} = \begin{bmatrix} \mathbf{R}_{ZYX}(\boldsymbol{\xi}_2)\boldsymbol{\upsilon}_1 \\ \mathbf{T}(\boldsymbol{\xi}_2)\boldsymbol{\upsilon}_2 \\ \frac{\mathbf{R}_{ZYX,3}(\boldsymbol{\xi}_2)T_B}{m} - \hat{\boldsymbol{\upsilon}}_2(\boldsymbol{\upsilon}_1 + \mathbf{W}_c) - \dot{\mathbf{W}}_c - g\mathbf{e}_3 - \frac{\mathbf{D}\dot{\boldsymbol{\xi}}_1}{m} \\ \mathbf{I}^{-1}(\boldsymbol{\tau}_B - \hat{\boldsymbol{\upsilon}}_2\mathbf{I}\boldsymbol{\upsilon}_2) \end{bmatrix}. \quad (10)$$

where [23]:

$$\dot{\mathbf{W}}_c = \nabla\mathbf{W}_c(\boldsymbol{\upsilon}_1 + \mathbf{W}_c) + \frac{\partial \mathbf{W}_c}{\partial t},$$

in which

$$\nabla\mathbf{W}_c = \mathbf{R}_{ZYX}(\boldsymbol{\xi}_2)\nabla\mathbf{W}\mathbf{R}_{ZYX}^T(\boldsymbol{\xi}_2);$$

$$\nabla\mathbf{W} = \begin{bmatrix} \frac{\partial W_X}{\partial x} & \frac{\partial W_Y}{\partial x} & \frac{\partial W_Z}{\partial x} \\ \frac{\partial W_X}{\partial y} & \frac{\partial W_Y}{\partial y} & \frac{\partial W_Z}{\partial y} \\ \frac{\partial W_X}{\partial z} & \frac{\partial W_Y}{\partial z} & \frac{\partial W_Z}{\partial z} \end{bmatrix}.$$

The model (10) is general with wind components in all directions; however, in this work, we are using it for the vertical

Preprint of the article: https://doi.org/10.1109/AIRPHARO52252.2021.9571054
Nekoo, Saeed Rafee, et al. "Experimental Investigation of Soft-Landing of Quadrotors via Induced Wind Modeling Approach." *2021 Aerial Robotic Systems Physically Interacting with the Environment (AIRPHARO)*. IEEE, 2021.

landing of multirotor UAVs. As a result, the wind vector is introduced as $\mathbf{W}(t) = \begin{bmatrix} 0 \\ 0 \\ V_{\mathrm{G}}(t) \end{bmatrix}$, where V_{G} is defined in Eq. (8).

III. Experimental Setup

A. Platform description

The experimental platform (Fig. 2) is a quadrotor with a customized protective case surrounding the propellers. The quadrotor platform, used in this work, is designed with cross configuration, using the DJI E305 as a motorization system supplied with a 4s LiPo battery. The weight of the UAV is 1.5 (kg) and the flight time is around 14 (min). The distance between the rotor's axis is 480 (mm) [33]. The employed autopilot of this setup is PX4.

Fig. 2. The experimental multirotor UAV.

B. Implementation

Commercial autopilots follow the scheme of linear cascade controllers (i.e. PX4 [34], DJI A3, and Ardupilot), However, to open a door to custom implementations they allow to be commanded by a companion computer through their Software Developer Kits (SDKs). Those SDKs can be commanded at different levels by passing one or more of their implemented controllers.

In this work, we aim to implement the soft-landing maneuver in a general way to validate the algorithm, minimize both the risk and the implementation time. Then, we directly bypass the first layer of the controller and send velocity commands to the autopilot.

The control of the translation and orientation is done separately in a commercial autopilot (i.e. PX4), so, we present a translational control since that considers the soft-landing approach in the system (10). The implementation strategy must embed the wind modeling inside the control law nonetheless, the attitude control inside the autopilot possesses PID structure:

$$\mathbf{u}(t) = \mathbf{K}_{\mathrm{P}}\mathbf{e}(t) + \mathbf{K}_{\mathrm{D}}\dot{\mathbf{e}}(t) + \mathbf{K}_{\mathrm{I}}\int_0^t \mathbf{e}(\tau)\mathrm{d}\tau, \tag{11}$$

where the three signals (components of $\mathbf{u}(t)$) will be used to construct the total thrust in the form of

$$T_{\mathrm{B}} = m\{[\mathbf{R}_{ZYX,3}(\boldsymbol{\xi}_2)]_1 u_1 + [\mathbf{R}_{ZYX,3}(\boldsymbol{\xi}_2)]_2 u_2 + [\mathbf{R}_{ZYX,3}(\boldsymbol{\xi}_2)]_3 (u_3 + g)\}. \tag{12}$$

where $[\mathbf{R}_{ZYX,3}(\boldsymbol{\xi}_2)]_1$ is the first component of the $\mathbf{R}_{ZYX,3}$. Then Eq. (12) is substituted into the system by $\mathbf{R}_{ZYX,3}(\boldsymbol{\xi}_2)\,T_{\mathrm{B}}/m$ which delivers the translation control signal. $\mathbf{K}_{\mathrm{P}} \in \mathbb{R}^{3\times3}$ is the constant proportional gain, $\mathbf{K}_{\mathrm{D}} \in \mathbb{R}^{3\times3}$ and $\mathbf{K}_{\mathrm{I}} \in \mathbb{R}^{3\times3}$ are the ones for derivative and integral parts, $\mathbf{e}(t)$, $\dot{\mathbf{e}}(t)$, and $\int_0^t \mathbf{e}(\tau)\mathrm{d}\tau$ are error vector, derivative and integral of that with respect.

If one assumes that the landing is almost vertical, the main parameters that reduce the thrust near the landing are acting in Z axis direction, or the third component of the control signal (11). Excluding the third element of the control law, one could present:

$$u_z(t) = K_{\mathrm{P},z}e_z(t) + K_{\mathrm{D},z}\dot{e}_z(t) + K_{\mathrm{I},z}\int_0^t e_z(\tau)\mathrm{d}\tau. \tag{13}$$

The constant gain $K_{\mathrm{P},z}$ defines the speed (vertical position variable) of the landing, also in collaboration with other derivative and integral parts. A proposed solution for practical implementation is to consider a state-dependent scalar gain $K_{\mathrm{P},z}(\mathbf{x})$ for thrust reduction near the ground based on the wind modeling approach. We define a feedforward reduction term

$$\mathbf{S}(\mathbf{x}) = -\hat{\boldsymbol{\upsilon}}_2(\boldsymbol{\upsilon}_1 + \mathbf{W}_{\mathrm{c}}) - \dot{\mathbf{W}}_{\mathrm{c}},$$

from translational dynamics (10), which reduces the thrust near the landing, presented in Fig. 3 for an arbitrary simulation.

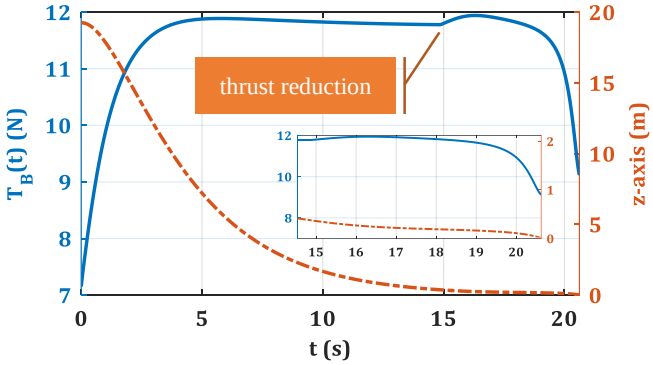

Fig. 3. Thrust reduction during soft-landing for a sample simulation due to feedforward thrust reduction.

If we substitute the third component of $\mathbf{S}(\mathbf{x})$, into the proportional gain of (13) with scaling factor α, we will find a new proportional gain as:

$$K_{\mathrm{P},z}(\mathbf{x}) = K_{\mathrm{P},z} + \alpha S_z(\mathbf{x}), \tag{14}$$

where α scales the $S_z(\mathbf{x})$ in the overall gain. So, observing (14), it can be realized that the gain is constant in all workspace, and $S_z(\mathbf{x})$ will be activated in $z_{\mathrm{c}} \in [0, 5R]$, reducing the $K_{\mathrm{P},z}(\mathbf{x})$ with tuning parameter α.

The tuning parameter α, was considered to enhance and weaken the effect of the soft-landing term, $S_z(\mathbf{x})$. Since the feed-

Preprint of the article: https://doi.org/10.1109/AIRPHARO52252.2021.9571054
Nekoo, Saeed Rafee, et al. "Experimental Investigation of Soft-Landing of Quadrotors via Induced Wind Modeling Approach." *2021 Aerial Robotic Systems Physically Interacting with the Environment (AIRPHARO)*. IEEE, 2021.

forward effect of the soft-landing mechanism was used in the experimental implementation, the precise value of α is not known and it should be defined by try and error and experimentation. It is obvious that selecting a large value for α results in positive feedback, or in other words, unstable control. That requires sensitivity in tuning. It would be ideal to implement the total system using a robust controller uniformly, similar to the theoretical design in Ref. [24], however, to present a practical implementation approach, and using a commercial autopilot, this proposed method has been employed.

IV. Results

Several trials have been performed for a vertical landing. The initial position of the drone was set at the height of $z = 2.5(\mathrm{m})$. The feedback on the position of the system was defined by the Opti-Track system. Using the algorithm to define $S_z(\mathbf{x})$ and then using the new gain $K_{\mathrm{P},z}(\mathbf{x})$ in (14), the results have been found. The regulation in Z axis direction is plotted in Fig. 4. To find the proper tuning parameter α, 5 tests have been performed, changing α from 0 to 1000. The best performance was gained by $\alpha = 750$. The landing of the drone in Z axis started by a constant speed, then near the ground for $\alpha = 0$, without soft-landing algorithm, the system touched the ground and bounced back with several bumps. The landing improved that eventually, $\alpha = 750$ gained the softest landing. Also, $\alpha = 1000$ caused instability in the system as we expected by positive feedback, presented in Fig. 4. This instability is limited to the landing phase near the ground, must be avoided by careful tuning before outdoor experiments. To address safety concerns, in an event of flying upward, after exiting the limit of $z_c(t) \in [0{,}5R]$, the soft-landing part is turned off.

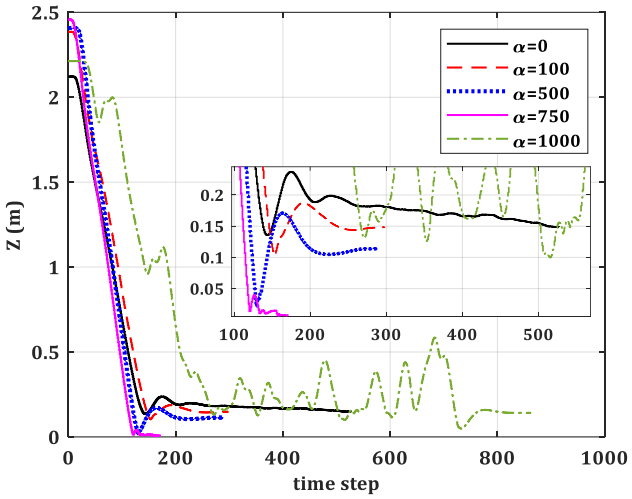

Fig. 4. The results of the soft-landing in Z axis direction with different selection of α.

V. Conclusions

This work investigated the soft landing problem for multirotor drones using a wind modeling approach, through an experimental study. The landing of a drone is a critical issue specifically in sensitive industrial sites such as refineries or places with explosive/flammable material. In those cases, hard contact will cause severe danger to the operation. The wind modeling approach introduces an augmented system by the velocity of the wind that could observe the effect of the wind on the system. Here the wind is produced by the drones' propellers and then that is reflected upward near the ground. The tendency to use commercial unmanned aircraft systems also limits the implementation flexibility, and therefore, complex algorithms are hard to be used. We proposed a method for the experimental implementation of the soft-landing on commercial autopilots with PD/PID controllers. Results showed successful landing on a testbed Opti-Track system.

Acknowledgments

This work is supported by the HYFLIERS project (HYbrid FLying-rolling with-snakE-aRm robot for contact inspection) funded by the European Commission H2020 Programme under grant agreement ID: 779411 (https://cordis.europa.eu/project/rcn/213049)] and by the ARTIC project funded by the Ministerio de Ciencia, Innovación y Universidades under the grant agreement ID: RTI2018-102224-B-I00.

References

[1] K. Tak and J. Kim, "Corrosion effect on inspection and replacement planning for a refinery plant," *Computers & Chemical Engineering*, vol. 117, pp. 97-104, 2018.
[2] https://www.oulu.fi/hyfliers/.
[3] C. Luo, W. Zhao, Z. Du, and L. Yu, "A neural network based landing method for an unmanned aerial vehicle with soft landing gears," *Applied Sciences*, vol. 9, p. 2976, 2019.
[4] A. Sahinoz, "Landing gear design and stability evaluation of a lunar lander for soft landing," in *Proceedings of the Bennett conference on mechanical engineering*, Pittsburgh, PA, USA, 2012, pp. 1-17.
[5] K. Zhang, P. Chermprayong, D. Tzoumanikas, W. Li, M. Grimm, M. Smentoch, *et al.*, "Bioinspired design of a landing system with soft shock absorbers for autonomous aerial robots," *Journal of Field Robotics*, vol. 36, pp. 230-251, 2019.
[6] K. Hang, X. Lyu, H. Song, J. A. Stork, A. M. Dollar, D. Kragic, *et al.*, "Perching and resting—A paradigm for UAV maneuvering with modularized landing gears," *Science Robotics*, vol. 4, 2019.
[7] L. Son, M. Surya, M. Bur, U. Ubaidillah, and R. Dhelika, "Shock and harmonic response analysis of UAV nose landing gear system with air damper," *Cogent Engineering*, vol. 8, p. 1905231, 2021.
[8] K. S. Peterson and A. G. Stefanopoulou, "Extremum seeking control for soft landing of an electromechanical valve actuator," *Automatica*, vol. 40, pp. 1063-1069, 2004.
[9] H. Yang and H. Baoyin, "Fuel-optimal control for soft landing on an irregular asteroid," *IEEE Transactions on Aerospace and Electronic Systems*, vol. 51, pp. 1688-1697, 2015.
[10] P. Mercorelli, "An antisaturating adaptive preaction and a slide surface to achieve soft landing control for

electromagnetic actuators," *IEEE/ASME Transactions on Mechatronics*, vol. 17, pp. 76-85, 2010.

[11] W. Myeong and H. Myung, "Development of a wall-climbing drone capable of vertical soft landing using a tilt-rotor mechanism," *IEEE Access*, vol. 7, pp. 4868-4879, 2018.

[12] K. Fricke, R. Giorgiani do Nascimento, and F. Viana, "Quadcopter soft vertical landing control with hybrid physics-informed machine learning," in *AIAA Scitech 2021 Forum*, 2021, p. 1018.

[13] J. S. Hayden, "The effect of the ground on helicopter hovering power required," in *Proc. AHS 32nd Annual Forum*, 1976.

[14] H. C. Curtiss, M. Sun, W. F. Putman, and E. J. Hanker, "Rotor aerodynamics in ground effect at low advance ratios," *Journal of the American Helicopter Society*, vol. 29, pp. 48-55, 1984.

[15] T. E. Lee, J. G. Leishman, and M. Ramasamy, "Fluid dynamics of interacting blade tip vortices with a ground plane," *Journal of the American Helicopter Society*, vol. 55, pp. 22005-22005, 2010.

[16] C. Powers, D. Mellinger, A. Kushleyev, B. Kothmann, and V. Kumar, "Influence of aerodynamics and proximity effects in quadrotor flight," in *Experimental Robotics*, 2013, pp. 289-302.

[17] P. J. Sanchez-Cuevas, G. Heredia, and A. Ollero, "Experimental approach to the aerodynamic effects produced in multirotors flying close to obstacles," in *Iberian Robotics Conference*, 2017, pp. 742-752.

[18] P. Sanchez-Cuevas, G. Heredia, and A. Ollero, "Characterization of the aerodynamic ground effect and its influence in multirotor control," *International Journal of Aerospace Engineering*, vol. 2017, 2017.

[19] X. Kan, J. Thomas, H. Teng, H. G. Tanner, V. Kumar, and K. Karydis, "Analysis of ground effect for small-scale UAVS in forward flight," *IEEE Robotics and Automation Letters*, vol. 4, pp. 3860-3867, 2019.

[20] G. Shi, X. Shi, M. O'Connell, R. Yu, K. Azizzadenesheli, A. Anandkumar, *et al.*, "Neural lander: Stable drone landing control using learned dynamics," in *2019 International Conference on Robotics and Automation (ICRA)*, Montreal, Montreal, Canada, 2019, pp. 9784-9790.

[21] J.-G. Juang, H.-H. Chang, and K. C. Cheng, "Intelligent landing control using linearized inverse aircraft model," in *Proceedings of the 2002 American Control Conference (IEEE Cat. No. CH37301)*, Anchorage, AK, USA, 2002, pp. 3269-3274.

[22] A. Betz, "The ground effect on lifting propellers," *Technical Memorandums, National Advisory Committee for Aeronautics, N. 836*, 1937.

[23] M. Lungu, "Backstepping and dynamic inversion combined controller for auto-landing of fixed wing UAVs," *Aerospace Science and Technology*, vol. 96, p. 105526, 2020.

[24] S. R. Nekoo, J. R. Acosta, G. Heredia, and A. Ollero, "Soft-landing of multi-rotor drones using a robust nonlinear control and wind modeling*," in *2021 International Conference on Unmanned Aircraft Systems (ICUAS)*, Athens, Greece, 2021.

[25] B. W. McCormick, "Aerodynamics aeronautics and flight mechanics," 2nd ed. New York NY: John Wiley & Sons Inc, 1995.

[26] I. C. Cheeseman and W. E. Bennett, "The effect of the helicopter rotor by ground on a forward flight," *Aeronautical Research Council Reports and Memoranda, No. 3021*, 1957.

[27] S. R. Nekoo, J. Á. Acosta, and A. Ollero, "Geometric control using the state-dependent Riccati equation: application to aerial-acrobatic maneuvers," *International Journal of Control*, pp. 1-13, 2021.

[28] S. R. Nekoo, J. Á. Acosta, A. E. Gomez-Tamm, and A. Ollero, "Optimized thrust allocation of variable-pitch propellers quadrotor control: A comparative study on flip maneuver," in *2019 Workshop on Research, Education and Development of Unmanned Aerial Systems (RED UAS)*, Cranfield, United Kingdom, United Kingdom, 2019, pp. 86-95.

[29] S. R. Nekoo, J. Á. Acosta, and A. Ollero, "Collision avoidance of SDRE controller using artificial potential field method: Application to aerial robotics," in *2020 International Conference on Unmanned Aircraft Systems (ICUAS)*, Athens, Greece, 2020, pp. 551-556.

[30] S. R. Nekoo, J. Á. Acosta, and A. Ollero, "Fully coupled six-DoF nonlinear suboptimal control of a quadrotor: Application to variable-pitch rotor design," in *Iberian Robotics conference*, 2019, pp. 72-83.

[31] F. Sabatino, "Quadrotor control: modeling, nonlinear control design, and simulation," *Master's Degree Project, KTH Electrical Engineering, Stockholm, Sweden*, 2015.

[32] P. R. Ambati and R. Padhi, "A neuro-adaptive augmented dynamic inversion design for robust auto-landing," *IFAC Proceedings Volumes*, vol. 47, pp. 12202-12207, 2014.

[33] P. J. Sanchez-Cuevas, G. Heredia, and A. Ollero, "Multirotor UAS for bridge inspection by contact using the ceiling effect," in *2017 International Conference on Unmanned Aircraft Systems (ICUAS)*, 2017, pp. 767-774.

[34] L. Meier, D. Honegger, and M. Pollefeys, "PX4: A node-based multithreaded open source robotics framework for deeply embedded platforms," in *2015 IEEE international conference on robotics and automation (ICRA)*, 2015, pp. 6235-6240.